Electronic States of a Novel Smaragdyrin Isomer: Polarized Spectroscopy and Theoretical Studies

A. Gorski,[†] B. Lament,[†] J. M. Davis,[‡] J. Sessler,*[,‡] and J. Waluk*[,†]

Institute of Physical Chemistry, Polish Academy of Sciences, Kasprzaka 44, 01-224 Warsaw, Poland and Department of Chemistry, Institute of Cellular and Molecular Biology, The University of Austin, Austin, Texas 77204-5641

Received: November 20, 2000; In Final Form: February 26, 2001

Spectral and theoretical techniques were applied to investigate the electronic structure and spectra of two recently synthesized pentapyrrolic macrocycles, isomers of smaragdyrin: 16,20-dibutyl-2,3,6,7,10,11,15,21-octamethyl-[22]pentaphyrin-(1.1.1.0.0) (**1**) and 16,20-dibutyl-2,3,6,7,10,11,15,21-octamethyl-5-oxa-[22]pentaphyrin-(1.1.1.0.0) (**2**). Combined use of linear dichroism, magnetic circular dichroism, fluorescence anisotropy and INDO/S calculations resulted in the location and assignments of a number of electronic transitions (eleven for **1** and seven for **2**). Even though the spectral pattern differs somewhat from that characteristic of most porphyrins, the results show that the four lowest excited electronic singlet states of both compounds are very well described by a four-orbital model, widely used for the interpretation of spectra in this type of compounds. Fluorescence and transient absorption/bleaching measurements enabled the determination of the rate constants of the radiative and nonradiative S_1 depopulation processes. These photophysical properties are consistent with a rigid, nearly planar excited state geometry that is essentially unchanged with respect to the ground-state structure.

1. Introduction

The enormous role played by porphyrin derivatives in crucial biological processes has provided a stimulus for the synthesis and study of various porphyrin-related compounds, such as constitutional isomers of porphyrin[1] and expanded porphyrins.[2] These investigations are gaining momentum due to prospects of future applications in many diverse areas, e.g., photodiagnostics and phototherapy,[3] material science,[4] and waste disposal.[5] All these fields combine the use of chemical substance and light; therefore, of utmost importance becomes the detailed characterization of electronic structure, and, in particular, the properties of the lowest excited states. Even for the parent compound porphyrin, this task has not yet been fully accomplished. The absorption spectra of porphyrin and many of its derivatives, reveal a characteristic pattern of two rather weak electronic transitions (Q-bands), followed, at higher energies, by two strong transitions (Soret bands). The exact location of the two Soret transitions in porphyrins and the possible presence of other, close-lying transitions still remain the subject of controversy.[6] The separation of the four lowest electronic transitions from other electronic states is due to the energy spacing of molecular orbitals. The two highest occupied ones (HOMO) lie much higher in energy than the third and lower MOs. Analogous behavior is observed for the first and second LUMOs, which are well-spaced from the higher-lying unoccupied orbitals. A consequence of such orbital energy ordering is that the four lowest excited singlet states can usually be quite satisfactorily described using a basis set of only four orbitals, the two HOMOs and the two LUMOs. The resulting "four-orbital model", first proposed by Gouterman,[7] has been widely used to interpret spectral properties of various porphyrinoids.

About a decade ago, when only one such compound existed, a simple MO analysis based on semiempirical calculations was performed for the various conceivable "nitrogen-in" synthetic isomers of porphyrin.[8] For all these constitutional isomers, the theory predicted that a description of absorption (and related properties, such as magnetic circular dichroism (MCD)) in terms of four-orbital model seemed justified. This has been experimentally confirmed for porphycene, the first known isomer of porphyrin, and for many of its derivatives,[9] as well as for the ethyl derivatives of two other recently synthesized porphyrin isomers, corrphycene and hemiporphycene.[10]

While the above is gratifying, our studies have also revealed that in several porphyrinoids more than four electronic states can be detected in the low energy region of the spectrum. For dibenzoporphycenes, we have observed an "intruder" state lying between the Q and Soret bands.[11] Studies of neutral and various protonated forms of substituted rosarin, a hexapyrrolic macrocycle, have shown that in this molecule at least six molecular orbitals, the three HOMOs and three LUMOs, have to be taken into account in order to obtain a reasonable description of the electronic absorption pattern.[12] In both cases, the larger number of electronic transitions was due to smaller MO energy separations.

In this work, we present the results of spectral, photophysical, and theoretical studies of two recently synthesized[13] porphyrinoids, isomers of smaragdyrin ([22]pentaphyrin(1.1.0.1.0)), namely 16,20-dibutyl-2,3,6,7,10,11,15,21-octamethyl-[22]pentaphyrin-(1.1.1.0.0) (**1**) and 16,20-dibutyl-2,3,6,7,10,11,15,21-octamethyl-5-oxa-[22]pentaphyrin-(1.1.1.0.0) (**2**) (Chart 1). The (*k.l.m.n.o*) nomenclature refers to the number of meso-carbons

* Corresponding author. E-mail: waluk@ichf.edu.pl. Fax: (+48) 391 20 238.
[†] Polish Academy of Sciences.
[‡] The University of Austin.

10.1021/jp004255a CCC: $20.00
Published on Web 05/01/2001

CHART 1: Formulas

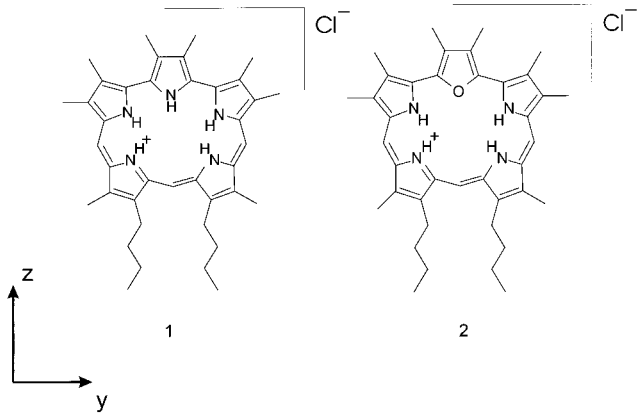

linking the adjacent pyrrole units. The aim of the spectral work was to determine the electronic structure of the two compounds, to assign the lowest electronic transitions and to relate them to those of porphyrin on the basis of both experiment and calculations. The photophysical studies were focused on ascertaining the efficiency of fluorescence and triplet formation, both parameters being crucial for possible applications in photodynamic therapy. Our investigation led to the location and assignment of a large number of electronic transitions. In particular, strong electronic transitions were observed in the vicinity of the Soret bands, their origin being described by orbitals other than the ones used in the Gouterman model. Nevertheless, an appropriately modified four orbital model proved to work extremely well in the description of the four lowest electronic states.

2. Experimental and Computational Details

The synthesis and purification of **1** and **2** have been described previously.[13] The results reported here are mostly for the protonated forms, since the neutral species turned out to be unstable. Still, it was possible to estimate some phophysical parameters for the neutral species, allowing qualitative comparisons to be made with the more reliable data for the protonated structures.

Spectral grade solvents, checked for the presence of fluorescing impurities, were used. Absorption spectra were recorded on a Shimadzu UV3100 spectrophotometer, equipped with a variable temperature cell. Steady state fluorescence and emission anisotropy spectra were obtained using an Edinburgh FS 900 CDT fluorometer (Edinburgh Analytical Instruments). Fluorescence excitation spectra were recorded at concentrations sufficiently low to ensure correspondence with the absorption. Fluorescence anisotropy was additionally measured on a Jasny spectrofluorometer.[14] The emission quantum yields were determined using quinine sulfate in 0.1 N H_2SO_4 ($\varphi_{fl} = 0.51$) as a standard.[15] Fluorescence decays were obtained on an Edinburgh FL 900 CDT time-resolved fluorometer (Edinburgh Analytical Instruments). Transient absorption spectra were recorded on a home-built instrument,[16] allowing a time resolution of 1 ns.

Linear dichroism (LD) measurements were performed on uniaxially oriented stretched samples of polyethylene (PE), containing small amounts of **1** or **2**. The compounds were introduced into PE by placing the powdered samples of **1** and **2** on a polymer sheet and gradually adding droplets of chloroform. After several hours, the film was carefully washed with methanol, to avoid formation of microcrystallites on the surface.

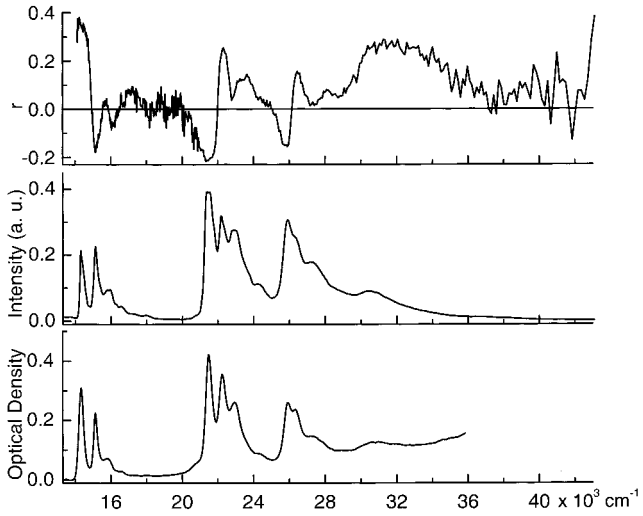

Figure 1. (Bottom) absorption, (middle) fluorescence excitation (arbitrary units, monitored at 14 300 cm^{-1}), and (top) anisotropy of fluorescence excitation of **1**. The spectra were measured at 77 K in EPA glass (ethyl ether:isopentane:ethanol 5:5:2).

Magnetic circular dichroism (MCD) spectra were measured on a JASCO J-715 spectropolarimeter, equipped with a home-built permanent magnet or an electromagnet. The values of the Faraday *B* terms were extracted from the isotropic solution spectra using the method of moments:

$$B = -33.53^{-1} \int d\tilde{\nu}\, [\Theta]_M/\tilde{\nu}$$

where $\tilde{\nu}$ is the wavenumber and $[\Theta]_M$ is the magnetically induced molar ellipticity per unit magnetic field (in units of deg L m^{-1} mol^{-1} G^{-1}).

Calculations of excited-state energies, oscillator strengths, and transition polarizations for **1** and **2** were performed using the INDO/S method.[17] Here, as input, we used either the X-ray[13] parameters or the AM1[18] optimized geometries. The 196 lowest singly excited configurations were taken into account in the CI procedure.

3. Results and Discussion

3.1. Spectroscopy and Calculations. Absorption spectra of **1** and **2** at 77 K are shown in Figures 1 and 2, respectively, while those taken at room temperature are presented in Figures 3 and 4. The spectral pattern is rich and quite different from that characteristic of porphyrin derivatives. Low-energy bands are located around 14 000−16 000 cm^{-1}, and are separated by about 7000 cm^{-1} from the onset of stronger transitions at higher energies. These two band systems may be considered analogues of Q and Soret transitions. However, in contrast to what is seen in porphyrins, the two band systems have comparable intensities, particularly in **1**. Several additional electronic transitions are observed above 26 000 cm^{-1}, again with intensities not much different from those of the strongest band system. This behavior is very different from that of porphyrins, wherein the Soret band intensity is much larger than that of all other electronic transitions.

An analysis of the absorption spectra with the help of polarized spectroscopy techniques reveals that each of the lowest three band systems starting at 14 200, 21 500, and 26 100 cm^{-1} in **1** and at 14 800, 22 400, and 25 600 cm^{-1} in **2** is composed of two close-lying electronic transitions, with the origins separated by less than 1000 cm^{-1}. The two components of each pair have different polarizations, as evidenced by the shape of

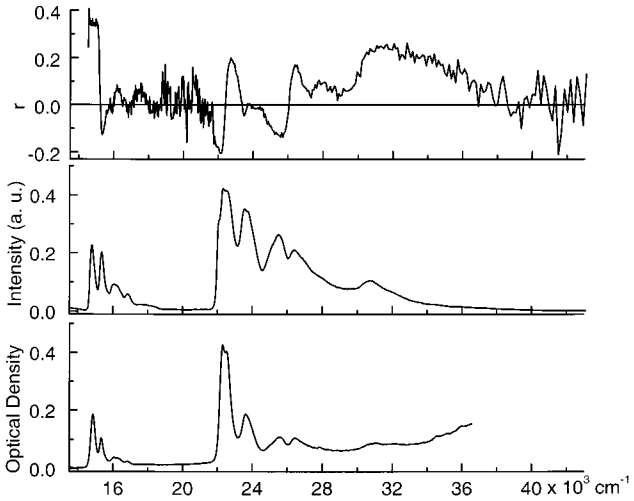

Figure 2. (Bottom) absorption, (middle) fluorescence excitation (monitored at 14 700 cm^{-1}), and (top) anisotropy of fluorescence excitation of **2** at 77 K in EPA glass.

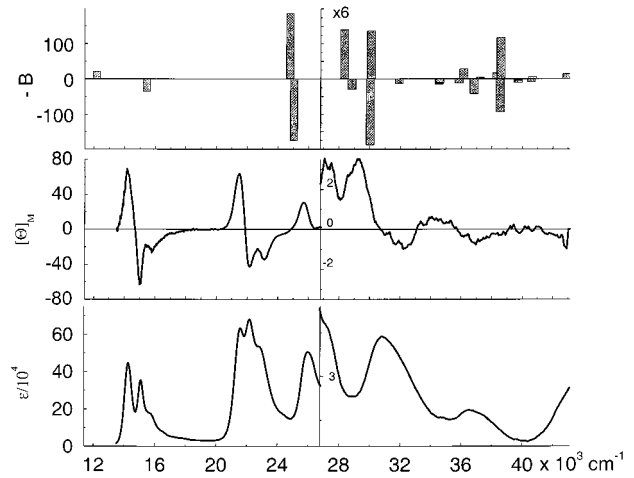

Figure 3. (Bottom) absorption, (middle) MCD spectrum of **1** in acetonitrile at 293 K, and (top) INDO/S calculated values of transition energies and *B* terms.

the anisotropy of fluorescence excitation curves for both compounds (Figures 1 and 2). Different polarizations make it possible to separate the vibronic components of each transition. In the lowest energy transistions, vibronic activity of a mode having a frequency of 1300−1600 cm^{-1} is observed for both compounds (Tables 1 and 2).

The moments of the second, third, and fifth transitions are practically orthogonal to the moment of the S_0-S_1 transition, as evidenced by the anisotropy values, close or equal to −0.2. On the other hand, a small value is obtained for the angle between the S_0-S_1 transition moment and the moments of the fourth and the sixth transitions. The observed positive values must be treated as lower limits, due to overlap with differently polarized close-lying transitions. These findings are consistent with an approximate C_{2v} symmetry for the chromophores. Indeed, X-ray diffraction analysis of both **1** and **2** reveals nearly planar structures, with only the middle pyrrole ring of the terpyrrole moiety (the one bisected by the plane of symmetry) tilted out of the plane formed by the four other rings. This tilt is 23.2° in the case of **1** and 21.2° in the case of **2**.[13]

The location of the electronic transitions were independently confirmed by MCD experiments (Figures 3 and 4). The maxima and minima on the fluorescence excitation anisotropy curves

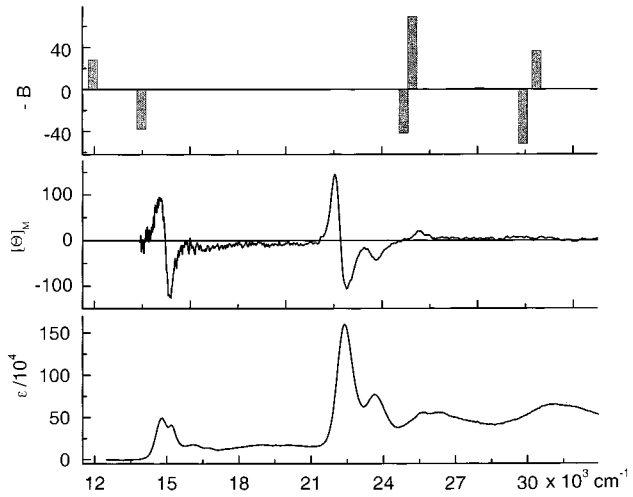

Figure 4. (Bottom) absorption, (middle) MCD spectrum of **2** in acetonitrile at 293 K, and (top) INDO/S calculated values of transition energies and *B* terms.

TABLE 1: Experimentally Determined Electronic Transition Energies of 1, along with the Corresponding Values of Fluorescence Anisotropy (*r*), Orientation Factors (K_i), and Faraday *B* Terms

	E (10^3 cm^{-1})	R	K_i [a]	B
1	14.3	0.36	0.44	−82
	15.8			
	17.3			
2	15.1	−0.18	0.35	99
	15.9			
	16.6			
	18.0			
3	21.5	−0.21	0.35	−55
	23.0			
	24.4			
4	22.2	0.25	0.44	74
	23.6			
5	25.9	−0.16	0.35	−26
	27.4			
6	26.5	0.15	0.44	
	28.1			
7	29.3	0.10		
8	30.6	0.25		
9	32.3	0.23		
10	34.1	0.24		
11	36.6	0.07		

[a] Accuracy: ±0.05.

coincide with the minima and maxima observed in the MCD spectra. Specifically, a −,+,−,+,− sequence of signs for the Faraday *B* terms is seen for the lowest four transistions in both compounds (it should be recalled that a positive MCD signal corresponds to a negative *B* term, and vice versa). Overall, the combination of MCD and fluorescence anisotropy makes it possible to identify eleven electronic transitions for **1** and seven for **2** (the lower number in the case of **2** is due to a weaker MCD signal in the region above 28 000 cm^{-1}, most probably caused by the overlap of positive and negative bands belonging to different electronic states). The transition energies, *B* terms, and the values of fluorescence anisotropies are given in Tables 1 and 2. For **1**, these tables also contain the values of orientation factors, K_i, obtained from the LD spectra. These parameters describe the average cosine square of the angle between a transition moment of the *i*th transition and the stretching direction of the polymer matrix that is used for recording the LD curves. A higher K_i value indicates a better average

TABLE 2: Experimentally Determined Electronic Transition Energies of 2, along with the Corresponding Values of Fluorescence Anisotropy (*r*) and Faraday *B* Terms

	E (10^3 cm^{-1})	r	B
1	14.8	0.36	−68
	16.2		
	17.6		
2	15.3	−0.13	73
	16.8		
	18.3		
3	22.1	−0.20	−65
	23.8		
4	22.5	0.20	111
	23.6		
5	25.6	−0.14	−26
	27.3		
6	26.4	0.17	
	27.8		
7	30.7	0.24	

alignment of the transition moment vector along the stretching direction. It has been shown that a correlation exists between the molecular shape and the degree of orientation: the molecules tend to align with their smallest cross section perpendicular to the stretching direction.[19] Thus, high values of K_i indicate transitions polarized close to the direction of the molecular long axis. The procedures that have been developed that make it possible to determine the absolute directions of the transition moments in the molecular frame, include a combination of the LD, fluorescence anisotropy and quantum-chemical calculations. This combined method is applicable even in the case of molecules of low symmetry (C_s, C_{2h}), where an infinite number of transition moment directions is possible.[20]

The K_i values were extracted from the LD spectra using the TEM (Thulstrup, Eggers and Michl) stepwise reduction procedure.[21] It is based on plotting linear combinations of both LD curves: E_Z, obtained for the electric vector of light polarized parallel to the polymer stretching direction, and E_Y, recorded with the electric vector perpendicular to it. K_i, the orientation factor for a transition i, is obtained from the curve for which a particular spectral feature (peak, shoulder) due to this transition disappears from the combination

$$1/2(1 - K_i)E_Z(\lambda) - K_iE_Y(\lambda) \qquad (1)$$

The LD spectra and the application of the TEM procedure are shown in Figures 5 and 6. The spectra are quite noisy, due to very low solubility of both compounds in PE. The K_i values span a rather narrow range. However, joint analysis of the LD and anisotropy measurements can be quite instructive. The first, fourth, and sixth electronic transitions in **1**, have $K_i = 0.44$, while for the other three (second, third, and fifth transitions) $K_i = 0.35$. This result is in perfect agreement with the fluorescence anisotropy data that show different polarizations in the two groups. Thus, the transitions with a larger K_i value are better aligned with the "effective orientation axis"—a direction which, on the average, orients the best. It is natural to identify the effective orientation axis with the long molecular direction z (vertical direction in Chart 1). This implies, given an approximate C_{2v} symmetry of the chromophore, that the first, fourth, and sixth electronic transitions in **1** are polarized along the z axis, while the moments of the second, third and fifth transitions coincide with the in-plane y axis, perpendicular to z.

For **2**, a reliable separation of the orientation factors for the components of each pair was not possible, due to the combination of low solubility in PE and the fact that the pairs of

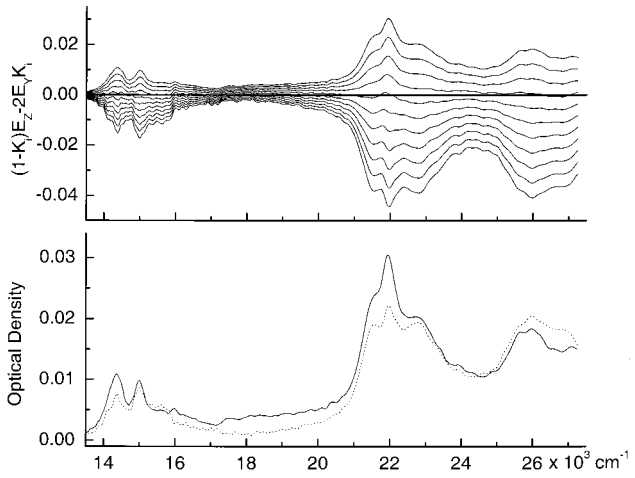

Figure 5. LD spectra of **1** (bottom) and the stepwise reduction procedure (top).

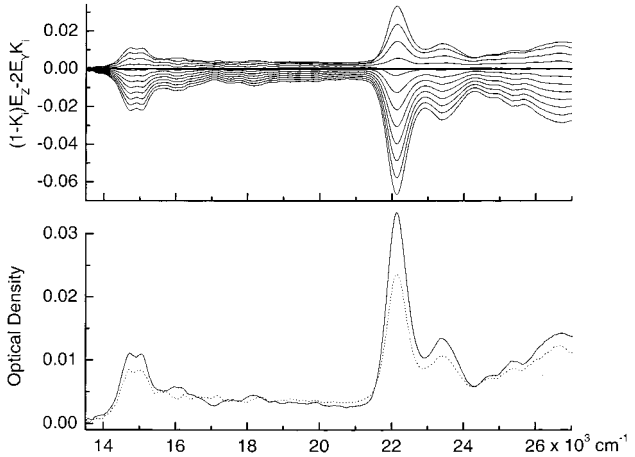

Figure 6. LD spectra of **2** (bottom) and the stepwise reduction procedure (top).

transitions 1−2, 3−4, and 5−6 lie even closer to each other than in **1**. Qualitative use of the reduction procedure for **2** yields an interesting result, namely that the lowest of the two peaks observed in the Soret region in PE (at 22 100 cm^{-1}) has a larger K_i value than the higher-lying peak (at 23 500 cm^{-1}). This is in contrast to the situation for **1**, wherein the first peak in the Soret region, located at 21 500 cm^{-1} in PE, has a smaller K_i value than the next peak at 21 900 cm^{-1}. This could mean that the ordering of the two Soret transitions is reversed in **2** with respect to **1**. While calculations support such a prediction (cf. Tables 3 and 4), this is probably not the case, since the −,+ pattern of the anisotropy signs remains the same in both compounds. Undoubtedly, the two transitions are nearly degenerate, and their overlap produces only one broad absorption band at room temperature; the two components become distinguishable only at lower temperatures (cf. Figures 2 and 4). This finding also explains why the extinction coefficient of the strongest absorption band is much larger in **2** than in **1**: In the former, it corresponds to a sum of two transitions. In addition, the oscillator strength of the strongest transition in **2** may be larger than in **1**, as predicted by calculations (Tables 3 and 4).

The results of calculations of transition energies, oscillator strengths, polarizations and Faraday B terms are presented in Tables 3 and 4. It can be seen that, at least for the low-lying transitions, the expected consequences of the approximate C_{2v} symmetry are indeed observed. The congruence between the

TABLE 3: Transition Energies, Oscillator Strengths (*f*), Polarizations, and Faraday *B* Terms Calculated for the Singlet States of 1[a]

state	*E* (10^3 cm^{-1})	*f*	α (deg)	*β* (deg)	*B*	main CI contribution
1	12.2	0.166	89	−2	−20.40	0.80 (1−1), 0.56 (2−2)
2	15.4	0.145	−2	−4	35.14	0.81 (2−1), 0.50 (1−2)
3	24.8	2.827	2	5	−183.41	0.84 (1−2), 0.48 (2−1)
4	25.0	2.737	−88	1	172.58	0.80 (2−2), 0.56 (1−1)
5	28.4	0.028	88	−1	−23.95	0.69 (1−4), 0.66 (2−3)
6	28.8	0.037	−3	8	5.36	0.61 (1−3), 0.54 (2−4)
7	30.0	0.178	89	0	30.78	0.77 (4−1), 0.45 (3−2)
8	30.1	0.003	48	−40	−22.19	0.77 (3−1)
9	31.9	0.053	−4	−14	2.42	0.85 (6−1)
10	32.2	0.001	−28	12	0.17	0.47 (7−1), 0.42 (5−1)
12	32.8	0.020	−89	2	−0.07	0.47 (2−3), 0.44 (5−1)
13	33.7	0.080	90	−8	1.94	0.69 (7−1), 0.35 (2−3)
17	36.8	0.059	88	6	7.61	0.58 (3−2), 0.46 (4−1)
18	37.2	0.091	−1	−20	−1.26	0.65 (1−6), 0.36 (5−2)
22	39.7	0.120	−39	24	1.17	0.42 (4−2), 0.35 (8−2)
23	39.7	0.093	27	24	1.24	0.48 (4−2), 0.38 (2−5)
24	40.6	0.037	−1	32	1.40	0.45 (1−1), 0.38 (5−2)
26	41.6	0.093	1	16	0.01	0.57 (9−2), 0.30 (1−6)
27	42.9	0.073	−89	−3	−2.62	0.54 (2−8), 0.33 (6−2)
28	43.4	0.019	−89	2	5.90	0.70 (1−6), 0.35 (2−6)
29	43.6	0.035	0	22	0.62	0.55 (1−10), 0.40 (2−7)
30	43.9	0.066	0	−14	−4.19	0.55 (2−7), 0.46 (1−8)
34	45.9	0.077	89	1	6.16	0.51 (8−2), 0.43 (2−8)

[a] Dominant configurations are shown using the convention of numbering the occupied orbitals as 1, 2, ... downward from the HOMO, and the unoccupied ones as −1,−2, ... upward from the LUMO. α is the angle between the the *z* axis and the projection of the transition moment in the *zy* plane. *β* describes the deviation of the transition moment from the *zy* plane (see Chart 1).

TABLE 4: Transition Energies, Oscillator Strengths (*f*), Polarizations, and Faraday *B* Terms for the Singlet States of 2[a]

state	*E* (10^3 cm^{-1})	*f*	α (deg)	*β* (deg)	*B*	main CI contribution
1	11.9	0.102	83	0	−28.19	0.75 (1−1), 0.58 (2−2)
2	14.0	0.086	−3	−4	37.80	0.77 (2−1), 0.55 (1−2)
3	24.9	2.960	−83	2	45.23	0.69 (2−2), 0.54 (1−1)
4	25.3	3.487	7	5	−72.55	0.71 (1−2), 0.48 (2−1)
5	27.7	0.000	56	−8	0.54	0.65 (2−3), 0.57 (1−4)
6	28.1	0.003	60	0	−1.30	0.60 (1−3), 0.54 (2−4)
7	29.9	0.264	−88	0	53.26	0.75 (4−1), 0.46 (3−2)
8	30.5	0.057	−1	−1	37.06	0.77 (3−1)
9	31.9	0.007	10	−19	0.26	0.72 (5−1)
10	32.6	0.011	15	−9	0.35	0.75 (6−1)
11	32.9	0.015	2	10	0.89	0.40 (2−4), 0.38 (7−1)
12	33.7	0.018	−73	−3	0.24	0.44 (5−1), 0.43 (2−4)
13	34.1	0.018	−49	47	0.85	0.52 (7−1), 0.36 (2−3)
16	36.8	0.025	−69	−12	3.37	0.44 (4−1), 0.40 (3−2)
19	38.4	0.063	−85	−2	−3.43	0.63 (1−5), 0.43 (6−2)
20	38.6	0.054	82	7	−3.01	0.58 (7−2), 0.39 (2−6)
21	39.0	0.129	−3	−27	10.39	0.60 (4−2), 0.47 (2−5)
22	39.5	0.058	−3	16	−2.99	0.43 (8−2), 0.39 (1−6)
27	42.7	0.045	−72	2	4.10	0.77 (1−7)
28	43.0	0.055	−68	5	−7.58	0.65 (2−8)
29	43.7	0.088	52	3	3.35	0.68 (2−7)

[a] See footnote to Table 3 for details.

experimentally observed transitions and the calculated ones is clear for the lowest two pairs, 1−2 and 3−4, although the energy ordering in the pairs is not always correct. This is not surprising, since the experimentally observed spacings between S_1-S_2 and S_3-S_4 transitions are less than 1000 cm^{-1}, while the accuracy of the INDO/S method is about 2000−3000 cm^{-1}. The leading configurations correspond to those predicted by the Gouterman's four-orbital model. A quantitative measure of how well a given state is described by this model is given by the sum of four CI coefficients corresponding to the electronic excitations from the two highest occupied molecular π orbitals to the two lowest unoccupied ones:

$$r = \sum_{ij=1,2} C_{ij}^{\,2} \qquad (2)$$

Values of *r* close to unity confirm the validity of this approach that is based on a simple 2 × 2 MO basis. The calculated values of *r* for **1** and **2** are given in Table 5. It is seen that the four orbital model works exceptionally well for both the Q and Soret transitions in the two compounds. The *r* values are about the same as in porphyrin,[11] or even higher in the case of one of the Soret transitions. Thus, for the S_1-S_4 states, the four configurations of the Gouterman model mix very little with other configurations. This is clearly seen in Figures 7 and 8, in which we compare transition energies and oscillator strengths calculated using various CI bases. The energy and intensity differences between a minimum 2 × 2 model and a corresponding calculation carried out using 196 (14 × 14) singly excited configurations are indeed very small. The reason the lowest four electronic states are so well described even by a 2 × 2 basis is due to the pattern of the MO energies. The two highest occupied orbitals are well-separated in energy, by about 2 eV, from the third and lower ones. The energy splitting between the second and third unoccupied orbital is also quite high, about 1.5 eV. This situation is analogous to that of porphyrin and porphycene, but very different from the orbital energy pattern in rosarin,[12] where the second and third highest occupied orbitals as well as the second and third lowest unoccupied ones were found to be very close in energy (for a high-symmetry idealized rosarin chromophore they are exactly degenerate).

TABLE 5: Calculated Values of the Coefficient *r* for the Lowest Excited States of 1 and 2[a]

	porphyrin			
	trans	cis	**1**	**2**
1	0.96	0.96	0.96	0.96
2	0.98	0.97	0.95	0.95
3	0.71	0.57	0.93	0.96
4	0.94	0.61	0.96	0.93
5			0.02	0.05
6			0.03	0.02

[a] See text for details. For comparison, data obtained for the trans and cis tautomeric forms of porphyrin[11] are also shown.

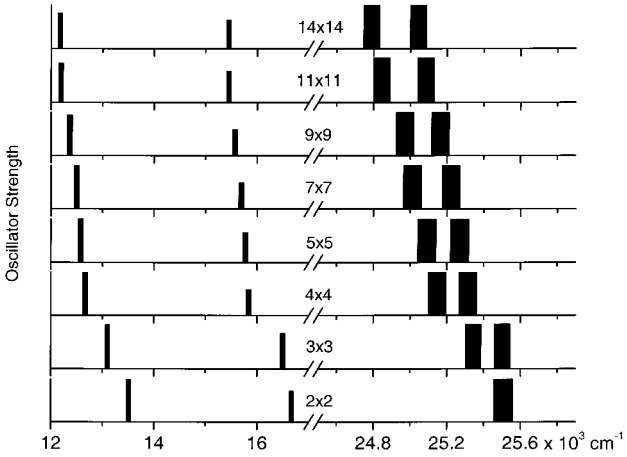

Figure 7. Calculated energies and intensities of the four lowest excited singlet states of **1** as a function of the CI basis size. The height of the bars is proportional to the oscillator strength; for the two lowest transitions it was expanded 10-fold.

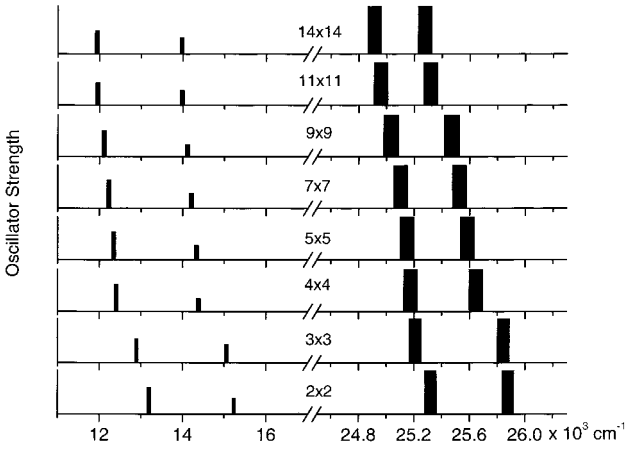

Figure 8. Calculated energies and intensities of the four lowest excited singlet states of **2** as a function of the CI basis size. See caption to Figure 7 for details.

Two important values arising from the calculations are the values of the energy splitting between the two highest occupied π orbitals (Δ**H**OMO) and that between the two lowest occupied π orbitals (ΔLUMO). The difference, ΔHOMO $-$ ΔLUMO, is crucial for the sign of the MCD in the region of the lowest four electronic transitions that can be described by the perimeter model,[21] i.e., via an approach closely related to that of Gouterman. The calculations predict that ΔHOMO $\ll$ ΔLUMO; for such a case, and for large values of D(L)/D(B), the ratio of dipole strengths of the Q and Soret transitions, a $+,-,+,-$ sequence of B terms is expected, as is indeed observed by experiment. A detailed analysis and the derivation of the relationship between ΔHOMO and ΔLUMO without resorting to calculations will be given in a separate work, wherein we compare the MCD spectra of **1** and **2** with those of another pentapyrrolic expanded porphyrin, sapphyrin.[22]

The values of ΔHOMO and ΔLUMO can also be used to estimate the relative intensities of the Q and Soret transitions. According to the perimeter model, the intensity ratio can be approximated as[9]

$$D(\mathrm{L})/D(\mathrm{B}) = (-1/4)[\Delta\mathrm{HOMO}^2 - \Delta\mathrm{LUMO}^2]/[E(\mathrm{B}) - E(\mathrm{L})]^2 \quad (3)$$

where E(B) $-$ E(L) is the energy difference between the B and L states of the parent perimeter. It can be replaced by the difference between the average energies of the Q and Soret transitions, about 7000 cm^{-1} in our case. For **1**, the calculations yield very small values of ΔHOMO, while ΔLUMO is about 1 eV. We thus obtain D(L)/D(B) $\approx$ 0.19, in very reasonable agreement with experiment. Another revealing analysis is to compare the experimental D(L)/D(B) intensity ratios in **1** and **2** with those predicted on the basis of orbital energy differences. In **2**, ΔLUMO is calculated to be smaller than in **1**. As a consequence, **2** should reveal a smaller D(L)/D(B) ratio, something that is indeed observed (cf. Figures 3 and 4).

Inspection of Tables 3 and 4 reveals that the transition moment directions are in accord with what would be expected given the approximate C_{2v} symmetry of the chromophore. This is in agreement with the results obtained from anisotropy measurements.

All the calculations presented above were made using the monoprotonated monocationic forms of the chromophores, without taking into account the effect, if any, of the chloride counterions. To investigate the possible influence of the chloride anion on the structure and spectral properties of **1** and **2**, we have made quantum chemical calculations of the transition energies, intensities and B terms for the overall neutral salt-like structures, wherein the chloride counterion is complexed above the center of the molecular plane of the positively charged chromophore. This geometry, optimized by the AM1 method, is in general agreement with the X-ray data.[13] Further, these INDO/S calculations reveal that the introduction of the chloride anion does not have a significant influence on the calculated spectral patterns.

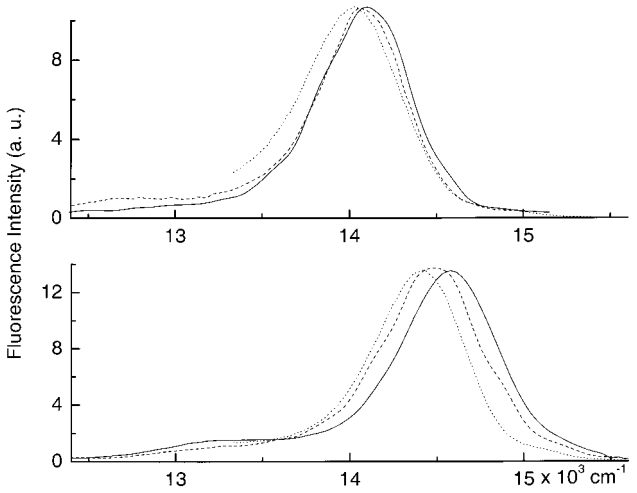

Figure 9. Room-temperature fluorescence spectra of **1** (top) and **2** (bottom) in different solvents: acetonitrile (solid line), methanol (dashed line), and cyclohexane (dotted line)

TABLE 6: Photophysical Parameters of 1 and 2

	solvent	ϕ_f [a]	ϕ_T [b]	τ_f, (ns)[c]	k_r (10^7 s^{-1})[d]	k_{ISC} (10^8 s^{-1})[e]	k_{IC} (10^8 s^{-1}) [f]
1	methanol	0.042	0.40	2.2 ± 0.2	1.9	1.8	2.5
	acetonitrile			2.5 ± 0.3			
	cyclohexane			2.8 ± 0.3			
2	methanol	0.046	0.47	1.4 ± 0.2	3.3	3.4	3.7
	acetonitrile			2.3 ± 0.2			
	cyclohexane			3.0 ± 0.2			

[a] Fluorescence quantum yield, accuracy: $\pm$20%. [b] Triplet formation efficiency; estimated accuracy: $\pm$30%. [c] Nondeaerated solutions; after deoxygenation, these values increase by about 10%. [d] The radiative constant corresponding to S_1 depopulation. [e] The rate constant for $S_1 \rightarrow T_1$ intersystem crossing. [f] The rate constant for $S_1 \rightarrow S_0$ internal conversion.

3.2. Photophysics. Fluorescence spectra for the monoprotonated forms of **1** and **2** in a nonpolar, polar aprotic and a protic solvent are shown in Figure 9. Selected photophysical parameters for these species are presented in Table 6. We have also attempted to characterize the neutral forms of **1** and **2**. Toward this end, NaOH or NH_3 were added to solutions of **1** and **2** in various solvents. This resulted in a blue shift of the fluorescence emission maximum by 8$-$10 nm. No appreciable change in intensity was observed. More comprehensive and precise investigations of the neutral forms of **1** and **2** turned out to be impossible because these forms proved unstable when exposed to light; indeed, they were seen to decay within hours.

Quantum yields for the formation of triplet states (φ_T) for **1** and **2** were calculated on the basis of transient absorption and bleaching measurements carried out on the nanosecond time scale (Figures 10 and 11). Briefly, the value of φ_T was estimated from the ratio of the amplitudes of the slow and fast kinetic signals describing the recovery of the ground-state population. The former amplitude corresponds to the $T_1 \rightarrow S_0$ intersystem

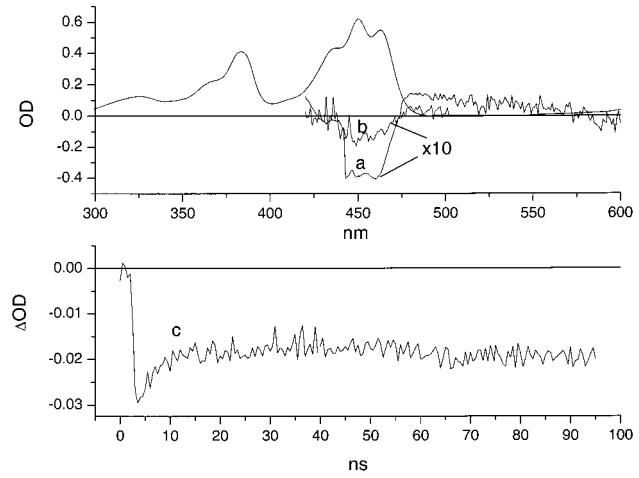

Figure 10. Top, stationary absorption and transient curves measured at the moment of excitation (a) and 50 ns after excitation (b). Bottom, kinetic curve of the ground-state repopulation of **1**, monitored at 450 nm (c).

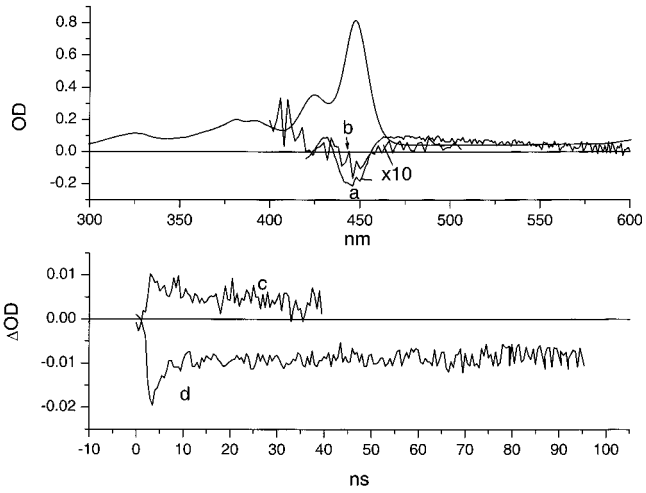

Figure 11. Top, stationary absorption and transient curves of **2** measured at the moment of excitation (a) and 40 ns after excitation (b). Bottom, transient signals, monitored at 470 nm (c) and at 440 nm (d).

crossing, while the latter, to direct $S_1 \rightarrow S_0$ internal conversion and emission channels. The experimental studies were performed at wavelengths where contributions from transient absorption are negligible. Alternatively, the $S_1 \rightarrow S_n$ and/or $T_1 \rightarrow T_n$ contributions could be subtracted from the transient signal. The lower portions of Figures 10 and 11 show the kinetic curves associated with ground-state repopulation; it was from those that the quantum yields of triplet formation could be determined.

The photophysical data shown in Table 6 provides support for the assigned "normal" character for the chromophores. The values of the rate constants for nonradiative depopulation are typical of aromatic compounds and do not point to considerable structural changes upon photoexcitation. This is in contrast to some other expanded porphyrins, such as rosarin, whose nonplanarity and conformational flexibility leads to a very efficient $S_1 \rightarrow S_0$ internal conversion process.[12] The smaragdyrin analogues, **1** and **2**, on the other hand, appear to retain their original planarity and rigidity in the lowest excited singlet state.

The rather high values of φ_T for **1** and **2**, combined with the strong absorption observed in the red region of the visible range could make these molecules potentially useful as photosensitizers for photodynamic therapy. However, the low stability of the neutral forms argues against such an application. On the other hand, the high stability of the protonated forms and the observation of anion binding in the solid state makes these species potentially attractive as optical anion sensors.

4. Summary and Conclusions

Combined use of various polarized spectroscopy techniques, namely, linear dichroism, fluorescence anisotropy, and magnetic circular dichroism has allowed many singlet electronic transitions in two isosmaragdyrin derivatives, specifically **1** and **2**, to be located and assigned. In particular, the location and absolute polarization of both components of the Q and Soret bands could be determined. Even though the absorption characteristics of **1** and **2** appear at first blush very different from those of porphyrin, both compounds were found to exhibit the "idealized" behavior of a system conforming to the classic four orbital model originally developed to interpret the spectral behavior of porphyrinoids. Application of a related approach, based on a perimeter model, allows details of the MCD pattern as well as the variations in the relative intensities of the Q and Soret transitions, to be readily understood.

We have previously shown that in some polypyrrolic macrocycles, such as rosarin, a CI basis set larger than used in the four orbital model is necessary. The finding that the electronic structure and spectra of isosmaragdyrins can be accounted for using a simpler orbital model than is needed for some other systems is quite reassuring for future studies of related chromophores, e.g., smaragdyrins and sapphyrins. A spectroscopic analysis of sapphyrins will be presented soon.[22]

Acknowledgment. Prof. J. Frelek from the Institute of Organic Chemistry of the Polish Academy of Sciences is greatly acknowledged for allowing us to use the JASCO spectropolarimeter. The technical assistance of G. Orzanowska is deeply appreciated. This work was supported in part by the National Science Foundation (grant CHE 9725399 to J.L.S.), The National Institute of Health (grant no. CA 68682 to J.L.S.), and by The Polish State Committee for Scientific Research (grant no. 3T01A 128 063 14).

References and Notes

(1) Sessler, J. L.; Gebauer, A.; Vogel, E. *The Porphyrin Handbook*, Kadish, K. M., Smith, K. M., Guillard, R., Eds.; Academic Press: San Diego, 2000; Vol. 2, Chapter 8.

(2) (a) Sessler, J. L.; Gebauer, A.; Weghorn, S. J. *The Porphyrin Handbook*; Kadish, K. M., Smith, K. M., Guillard, R., Eds.; Academic Press: San Diego, 2000; Vol. 2, Chapter 9. (b) Sessler, J. L.; Weghorn, S. J. *Expanded, contracted and isomeric porphyrins*; Organic Chemistry Series; Pergamon: New York, 1997; Vol. 15.

(3) (a) Harriman, A.; Maiya, B. G.; Murai, T.; Hemmi, G.; Sessler, J. L.; Mallouk, T. E. *J. Chem. Soc., Chem. Commun.* **1989**, 314. (b) Henderson, B.; Dougherty, T. J. *Photochem. Photobiol.* **1992**, *55*, 145. (c) Henderson, B., Dougherty, T. J., Eds. *Photodynamic Therapy: basic principles and clinical applications*; Marcel Dekker: New York, 1992.

(4) (a) Wagner, R. W.; Lindsey, J. S. *Pure Appl. Chem.* **1996**, *68*, 1373. (b) Wagner, R. W.; Lindsey, J. S.; Seth, J.; Palaniappan, V.; Bocian, D. F. *J. Am. Chem. Soc.* **1996**, *118*, 3996.

(5) (a) Sessler, J. L.; Burrel, A. K. *Topics Curr. Chem.* **1991**, *161*, 111. (b) Jasat, A.; Dolphin, D. *Chem. Rev.* **1997**, *97*, 2267.

(6) (a) Tretiak, S.; Chernyak, V.; Mukamel, S. *Chem. Phys. Lett.* **1998**, *297*, 357. (b) Baker, J. D.; Zerner, M. C. *Chem. Phys. Lett.* **1990**, *175*, 192. (c) Nakatsuji, H.; Hasegawa, J.; Hada, M. *J. Chem. Phys.* **1996**, *104*, 2321. (d) Gwaltney, S. R.; Bartlett, R. J. *J. Chem. Phys.* **1998**, *108*, 6790. (e) Serrano-Andrés, L.; Merchán. M.; Rubio, M.; Roos, B. O. *Chem. Phys. Lett.* **1998**, *295*, 195.

(7) (a) Gouterman, M. *J. Mol. Spectrosc.* **1961**, *6*, 138. (b) Gouterman, M.; Wagniere, G. H.; Snyder, L. C. *J. Mol. Spectrosc.* **1963**, *11*, 108.

(8) Waluk, J.; Michl, J. *J. Org. Chem.* **1991**, *56*, 2729.

(9) Waluk, J.; Müller, M.; Swiderek, P.; Köcher, M.; Vogel, E.; Hohlneicher, G.; Michl, J. *J. Am. Chem. Soc.* **1991**, *113*, 5511.

(10) Gorski, A.; Vogel, E.; Waluk, J. Manuscript in preparation.
(11) Dobkowski, J.; Galievsky, V.; Starukhin, A.; Vogel, E.; Waluk, J. *J. Phys. Chem. A* **1998**, *102*, 4996.
(12) Lament, B.; Dobkowski, J.; Sessler, J. L.; Weghorn, S. J.; Waluk, J. *Chem. Eur. J.* **1999**, *10*, 3039.
(13) Sessler, J. L.; Davis, J. M.; Lynch, V. *J. Org. Chem.* **1998**, *63*, 7062.
(14) Jasny, J.; Waluk, J. *Rev. Sci. Instrum.* **1998**, *99*, 2242.
(15) Velapoldi, R. A. *Natl. Bur. Stand. 378, Proc. Conf. NBS* **1972**, 231.
(16) Jasny, J.; Sepioł, J.; Karpiuk, J.; Gilewski, J. *Rev. Sci. Instrum.* **1994**, *65*, 3646.
(17) Ridley, J. E.; Zerner, M. Z. *Theor. Chim. Acta* **1973**, *32*, 111.
(18) Dewar, M. J. S.; Zoeblisch, E. G.; Healy, E. F.; Stewart, J. J. P. *J. Am. Chem. Soc.* **1985**, *107*, 3902.
(19) Michl, J.; Thulstrup, E. W. *Spectroscopy with Polarized Light*; VCH Publishers: New York, 1995.
(20) Waluk, J.; Thulstrup, E. W. *Chem. Phys. Lett.* **1987**, *135*, 515. Spanget-Larsen, J.; Waluk, J.; Thulstrup, E. W. *J. Phys. Chem.* **1990**, *94*, 1800. Spanget-Larsen, J.; Waluk, J.; Eriksson. S.; Thulstrup, E. W. *J. Am. Chem. Soc.* **1992**, *114*, 1942.
(21) Michl. J. *J. Am. Chem. Soc.* **1978**, *100*, 6801, 6812, 6819.
(22) Lament, B.; Gorski, A.; Sessler, J.; Michl, J.; Waluk, J. Manuscript in preparation.